International Journal of Multiphase Flow xxx (xxxx) 104685

Contents lists available at ScienceDirect

International Journal of Multiphase Flow

journal homepage: www.elsevier.com/locate/ijmulflow

A numerical study on sedimentation effect of dust, smoke and traffic particle deposition in a realistic human lung

Md. M. Rahman [a, b, *], Ming Zhao [a, *], Mohammad S. Islam [c], Kejun Dong [a], Suvash C. Saha [c]

[a] School of Engineering, Design and Built Environment, Western Sydney University, Penrith, NSW 2751, Australia
[b] Department of Mathematics, Faculty of Science, Islamic University, Kushtia-7003, Bangladesh
[c] School of Mechanical and Mechatronic Engineering, University of Technology Sydney, Ultimo, NSW 2007, Australia

ARTICLE INFO

Keywords:
Airflow
Pollutant particles
Human lungs
Drug delivery
Sedimentation effect
Physical activity
Deposition mechanism

ABSTRACT

Inhalation of pollutants can be deadly for respiratory health, as toxic pollutants can penetrate the deep lungs which could occur severe respiratory infection and lead to life-threatening respiratory diseases. The excessive presence of pollutants in the environment increases the concern of potential respiratory health hazards. To date, a microscopic understanding of the sedimentation effect on dust, smoke and traffic (pollutant) particles transported to the airways is missing in the literature. This first-ever study aims to analyse the sedimentation effect in various directions of pollutant particle transport in airways. This study also quantitatively explains how particle size, density, and physical exercise impact pollutant particle transport and deposition (TD) in the human lung airways. The contribution of the sedimentation effect is largely independent of particle size. The sedimentation effect can also be found significant at the trachea region when the fluid flow is horizontal. Overall, traffic particles with large diameters and high flow rates are deposited in the upper lung, whereas dust particles with large diameters and high flow rates are deposited in the deep lung. It is expected that 79.1 % of the particles will reach the deep lung. The difference between the deposition rates of the horizontal and vertical lungs reduces if the particle size reduces, the flow rate increases or the particle density reduces. The deposition rate of a horizontal lung for the heaviest particles (traffic) at 15 L/min flow rate is about 4.5 % higher than that of a vertical lung with the same flow rate.

1. Introduction

Human health, particularly the respiratory system, is greatly impacted by pollutant particles or particulate matter (PM), which is a big public health concern (Valavanidis et al., 2008). Pollutant particles can enter the human lungs thoroughly, circulate in the blood, and then impact other cells and tissues (Chen et al., 2016). Asthma, lung cancer, and chronic obstructive pulmonary disease are among the most common respiratory diseases due to the inhalation of pollutants particles (Kyung and Jeong, 2020). PM has been responsible for morbidity and mortality in people all over the world. According to the World Health Organization (WHO), 8 million people died each year due to pollutant particles, and 9 out of 10 people are affected by pollutant particles globally (Organization, 2009). Nearly 47 % of deaths were attributed to lung diseases, including 7–8 % from lung cancer, 19 % from chronic obstructive pulmonary disease, and 21 % from pneumonia (Tekatli et al., 2016).

Pollutant-related particle emission has become a major concern in recent years due to the significant risk that it causes to human health (Verhoeven et al., 2021). After inhalation, coarse dust particles (>10 μm) typically settle in the upper respiratory system. The pulmonary alveoli ultimately become deposited with the smaller (≤4 μm) dust particles, resulting in chronic lung disease (Derbyshire, 2007). Moreover, cigarette smoke particles (CSP) cause significant damage to human lungs. Smoking and other tobacco products contain about 7000 compounds, of which 250 are harmful to people (Interventional et al., 2007). Smoke is still a major contributor to death and disability across the world (Nomura et al., 2022). In addition, most traffic particles are produced by diesel and compressed natural gas (CNG) engines (Agarwal et al., 2018). Coughs, itchy, and neuropsychiatric symptoms like headache, vomiting, nausea, difficulty breathing, chest constriction, and wheezing can all result from exposure to traffic particles (Oravisjärvi et al., 2011).

On the other hand, it is crucial to understand the particle transport dynamics and deposition process in human lung airways to improve the

* Corresponding authors at: School of Engineering, Design and Built Environment, Western Sydney University, Penrith, NSW 2751, Australia.
E-mail addresses: mdmizanur.rahman@math.iu.ac.bd (Md.M. Rahman), m.zhao@westernsydney.edu.au (M. Zhao).

https://doi.org/10.1016/j.ijmultiphaseflow.2023.104685
Received 5 August 2023; Received in revised form 15 October 2023; Accepted 22 November 2023
0301-9322/© 20XX

effectiveness of drug delivery for local lung diseases (Thakur et al., 2020). Pourmehran et al. (2016 conducted research on magnetic drug targeting using a human tracheobronchial airway model. The findings indicate great potential for magnetic drugs targeting enhancing deposition at the left lung area. Pourmehran et al. (2015) used Lagrangian magnetic particle tracking to simulate the targeting of magnetic drugs through the tracheobronchial airways. The results showed that the magnetic field improves particle deposition efficiency in a particular location. The literature has also reported on the effectiveness of the acoustic delivery of drugs to the maxillary sinus (Pourmehran et al., 2021; Pourmehran et al., 2020). The results demonstrate that increased stimulation amplitude significantly raises the aerosol deposition concentration in the maxillary sinus. In order to evaluate the effectiveness of drug delivery, it is important to understand the mechanism of particle deposition in human lung airways (Lee et al., 2018). Numerous academics have used CFD to characterise particle deposition in human lungs (Deng et al., 2019; Kleinstreuer and Zhang, 2003; Rahman et al., 2022b). The inhaled airborne particles or pharmaceutical aerosols are transferred and deposited in human respiratory systems based on the inertial impaction, gravitational sedimentation, and Brownian diffusion mechanism (Darquenne, 2020). The contributions of various processes to particle deposition in local airway segments depend on adequate particle size, density, local airflow rate, and gravity angle (Islam et al., 2022b). Sedimentation is typically significant for micron particles in the lower airways and alveolar areas, where the Reynolds numbers are low (Kleinstreuer and Zhang, 2010). There are hardly any direct laboratory investigations of the effect of gravitaty in particle deposition in human respiratory systems. Regional deposition fractions (DFs) are only included in published data in the alveolar region, where sedimentation may be predominant or happens in conjunction with diffusion and impaction (Kleinstreuer et al., 2007).

A number of studies were conducted to support the theory of particle deposition and transportation in the lung via an inhalation process. However, the literature lacks precise knowledge of the sedimentation effect on pollutant (dust, smoke and traffic) particle transport and deposition in a human lung. In order to evaluate the health risks associated with particle exposure from various sources, this research aims to quantify the sedimentation effect on pollutant particle deposition in human lungs with a range of densities and sizes under different breathing conditions. We also identified the vertical and horizontal contributions of the sedimentation effect. Additionally, a comprehensive investigation of this first-ever sedimentation effect in various directions will offer a quantitative understanding of how particle size, density, and physical exercise impact pollutant particle TD in the human lung airways.

Nomenclatures

P	fluid pressure	ρ	air density
T	fluid temperature	ρ_p	particle density
D	hydraulic diameter	μ	molecular viscosity
S_t	Stokes number	Δt	particle time step
Q_{in}	flow rate	G_i	Gaussian random number
u_i^p	particle velocity	S_0	spectral intensity function
d_p	particle diameter	ν	kinematic viscosity
u_i	fluid velocity	K_B	Boltzmann number
Re_P	particle Reynolds number	C_c	Stokes–Cunningham
F_{Di}	drag force	λ	gas molecules' mean free path
F_{gi}	gravitational force	d_{ij}	deformation tensor
F_{Bi}	Brownian force	η_d	deposition efficiency
F_{Li}	Saffman's lift force	U_τ	friction velocity
C_D	Drag coefficient	τ_w	wall shear stress
u_0	Fluid inlet velocity	η_e	escaping rate
g	Gravity acceleration	η	deposition efficiency rate

2. Numerical method

The primary determinants of particle deposition in human lung airways are breathing rhythm, particle shape, and particle size (Farkas et al., 2022). Inertia impaction and gravitational sedimentation play important roles when the particle size is on the microscale (Deng et al., 2018). However, many studies on microparticle TD in human lungs concentrate only on impaction mechanisms (Naseri et al., 2017; Rahman et al., 2021b; Zhang et al., 2002). We have considered the combination of inertia impaction, gravitational sedimentation, and diffusion effect in the current study.

2.1. Reconstructed anatomical model

The human respiratory tract has been reconstructed from CT scan images using three main techniques: detecting the inner wall points of the air routes, incorporating the inner wall points into rings with MIMICS software, and rebuilding the exterior wall of the air passages. The rings should then be stacked one on top of the other at the same distance as the CT slices. Finally, surfaces for the inner walls are built up around the circles. Hence, the digitised CT scan-based three-dimensional (3D) anatomical sixth-generation realistic lung is generated, which includes the mouth-throat region and the tracheobronchial upper lung airways in Fig. 1. The lung model is divided into four parts: mouth-throat, Larynx, Trachea and Bronchioles, as shown in Fig. 1, to make it easier to explain Particle TD in the discussion. A coordination system is defined with its x-direction pointing to the back of the lung and z-direction pointing upward, as seen in Fig. 1. Two scenarios are considered: (1) a vertical lung for a person who either stands or sits down and (2) a horizontal lung that represents a person who is lying down on his/her back. The direction of gravity of the above two scenarios is in the negative z- and positive x-directions, respectively. Because of the difference in the direction of gravity, the sedimentation effects caused by gravity in vertical and horizontal lungs will be different from each other.

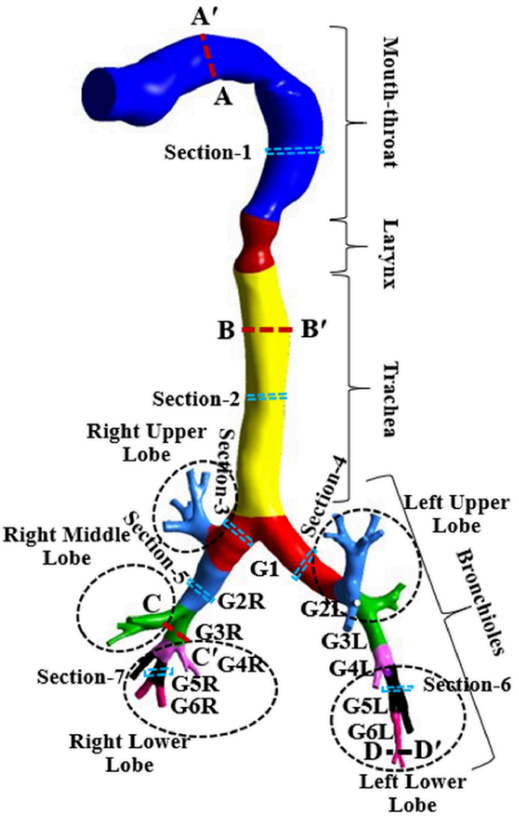

Fig. 1. Reconstruction of realistic mouth-throat and tracheobronchial lung airways.

2.2. Airflow model

To solve the airflow and particle TD in the lung airways, we used the ANSYS FLUENT (version 2022 R2) software. The Reynolds-averaged Navier-Stokes (RANS) equations perform as the governing equations for modelling the flow:

$$\frac{\partial \rho}{\partial t} + \frac{\partial}{\partial x_i}\left(\rho u_i\right) = 0 \tag{1}$$

$$\frac{\partial}{\partial t}\left(\rho u_i\right) + \frac{\partial}{\partial x_j}\left(\rho u_i u_j\right) = -\frac{\partial p}{\partial x_i} + \frac{\partial}{\partial x_j}\left[\mu\left(\frac{\partial u_i}{\partial x_j} + \frac{\partial u_j}{\partial x_i}\right)\right] + \frac{\partial}{\partial x_j}\left(-\rho\overline{u_i' u_j'}\right) \tag{2}$$

where t is time, x_i (i=1,2 and 3) are the Cartesian coordinates, u_i is the fluid velocity in the x_i-direction, p is the fluid pressure, ρ is the air density, and μ is the molecular viscosity. $\rho\overline{u_i' u_j'}$ on the right-hand side of equation (2) stands for the Reynolds stress.

The RANS equations are solved together with the shear stress transport (SST) k-ω turbulent model, which has been shown to be able to estimate the flow of complex lung geometries with high accuracy (Tretiakow et al., 2021). The pressure-velocity coupling and second-order upwind methods of FLUENT are used to solve the RANS equations. The lung model has a uniformly distributed constant velocity at its inlet and zero gauged pressure at all outlets (Naseri et al., 2014). With a non-slip boundary condition, the airway walls are considered smooth, stationary, and at rest (Islam et al., 2022a).

2.3. Particle transport model

Two-way models that take particle-particle interaction into consideration are required when the particle volume concentration exceeds 15 %. The volume concentration is, nonetheless, less than 15 % in any drug delivery and pollutant particle application (Dockery and Pope, 1994; Wong et al., 2012). In order to replicate the movement of diluted, suspended particles in the human lung, collision-free circumstances can be employed, or particle-particle contact can be removed (Farnoud et al., 2020). When the particle suspension entering the tracheobronchial airway is dilute, the particle-particle interaction (two-way coupling) can be ignored (Rahimi-Gorji et al., 2015). Hence, the current particle TD model is a one-way coupling model that considers particle movement caused by airflow but ignores the impact of particles on the airflow (Kuga et al., 2023). Every single particle's equation of motion is presented as (Inthavong et al., 2011):

$$\frac{du_i^p}{dt} = F_{Di} + F_{gi} + F_{Bi} + F_{Li} \tag{3}$$

where F_{Di}, F_{gi}, F_{Bi} and F_{Li} are the drag force, gravitational force, Brownian force, and Saffman's lift force per unit mass, respectively, and u_i^p is particle velocity in the x_i-direction. The gravitational force is calculated using the approach described below.

$$F_{gi} = \left(\frac{\rho_p - \rho}{\rho}\right) g \tag{4}$$

where ρ_p stands for particle density and g for gravity acceleration. The following formula is used to determine the drag force:

$$F_{Di} = \frac{18\mu}{\rho_p d_p^2} C_D \frac{Re_p}{24}\left(u_i - u_i^p\right) \tag{5}$$

where $Re_p = \rho d_p \left|u_i^p - u_i\right| / \mu$ and the drag coefficient C_D for the spherical particles is calculated by (Morsi and Alexander, 1972):

$C_D = a_1 + \frac{a_2}{Re_p} + \frac{a_3}{Re_p^2}$ for $0<Re_p<10$. where a_1, a_2, a_3 are functions of the Reynolds number Re_P given by:

$$a_1,\ a_2,\ a_3 = \begin{cases} 0,\ 24,\ 0 & 0 < R_e < 0.1 \\ 3.690,\ 22.73,\ 0.0903 & 0.1 < R_e < 1 \\ 1.222,\ 29.17,\ 3.89 & 1 < R_e < 10 \\ 0.617,\ 46.50,\ -116.67 & 10 < R_e < 100 \\ 0.364,\ 98.33,\ -2778 & 100 < R_e < 1000 \\ 0.357,\ 148.62,\ -47500 & 1000 < R_e < 5000 \\ 0.46,\ -490.546,\ 578700 & 5000 < R_e < 10000 \\ 0.519,\ -1662.5,\ 5416700 & R_e > 10000 \end{cases}$$

When molecules engage with one another, random, uncontrollable movement of the fluid's particles is known as Brownian motion (Torrens and Castellano, 2018). The definition of a Brownian motion is:

$$F_{Bi} = G_i\sqrt{\frac{\pi S_0}{\Delta t}} \tag{6}$$

where G_i is a Gaussian random number with unit variance and zero mean, Δt denotes the particle time step, and S_0 denotes the spectral intensity function corresponding to the diffusion coefficient by:

$$S_0 = \frac{216\nu k_B T}{\pi^2 \rho_p d_p^2 \left(\frac{\rho_p}{\rho}\right)^2 C_c} \tag{7}$$

where ν is the kinematic viscosity, $K_B = 1.380649 \times 10^{-23}$ J/Kis the Boltzmann constant, $T = 300K$ is the absolute fluid temperature, and C_c is the Stokes-Cunningham slip correction coefficient as

$$C_c = 1 + \frac{2\lambda}{d_p}\left(1.257 + 0.4e^{-\left(\frac{1.1 d_p}{2\lambda}\right)}\right) \tag{8}$$

where the mean free route (λ) of the gas molecules is 65 nm (Kuga et al., 2023). The following formula is used to determine the lift force of Saffman:

$$F_{Li} = \frac{2K\nu^{\frac{1}{2}}\rho d_{ij}}{\rho_p d_p \left(d_{lk} d_{kl}\right)^{\frac{1}{4}}}\left(u_j - u_j^p\right) \tag{9}$$

where, $K = 2.594$ is the constant coefficient of Saffman's lift force and $d_{ij} = \left(\partial u_i/\partial x_j - \partial u_j/\partial x_i\right)/2$ is the deformation tensor of the flow velocity.

In the simulations, 157000 spherical particles are randomly released at once on the inlet boundary or mouth surface. For particle deposition, a "trap" condition is implemented on the airway walls, and an "escape" condition is implemented at the outlets (Rahimi-Gorji et al., 2016). The particles can travel through the output boundary in the escape condition without being reflected back. Particles that collide with the inner surface of the lung airways are trapped under the trap location. As the airway walls contain mucus, which is very sticky, this "trap" condition is adequate.

2.4. Particle deposition efficiency calculation

Deposition efficiency is the percentage of particles absorbed (trapped) on the interior surfaces of the human lung airways, and it is measured by:

$$\text{Deposition efficiency, } \eta(\%) = \frac{\text{The number of particles deposited in a g}}{\text{Total number of particles inhaled through}}$$

3. Grid dependency study and model validation

3.1. Mesh generation and mesh dependency study

The computational mesh in various locations of the lung model is depicted in Fig. 2(a) to (d), including the asymmetric mouth-throat region, the bronchioles section, and a portion of the lung airways. The mesh's quality plays a significant role in the CFD study of any computational difficulty. The orthogonal quality of a mesh identifies its quality, and a good mesh indicates if the orthogonal quality maximum values are smaller than 1. The value is calculated using the Ansys Workbench 2022 R2 Solver, which yields a maximum orthogonal quality of 0.997. The Ansys-Mesh Modeller's patch-independent approach is used to generate the grid. The volume grid is constructed using structured tetrahedral elements, while the surface meshing is generated using triangular mesh due to the curved surface of the respiratory passages. The boundary layer flow was precisely simulated by ten-layer smooth inflation very near the walls (Fig. 2b). For the high resolution of complex flows at carinal angles (Fig. 2d), denser meshes are employed.

Six mesh sizes are used to conduct the grid independency test, and their node numbers are 705523 (Mesh-1), 836186 (Mesh-2), 1001916 (Mesh-3), 1285635 (Mesh-4), 1615161 (Mesh-5) and 2026697 (Mesh-6). Near the wall, the densest mesh has a grid size of 0.1 mm, and the mesh size is inversely proportional to the element count. For the three sections denoted in Fig. 3(a), the average velocities are shown in Fig. 3 (b)–(d), where X is the position along the section diameter. It can be shown that if the mesh is denser than Mesh-4, increasing the grid number has little effect on velocity. The largest deference in velocity between Mesh-5 and Mesh-6 is approximately 0.01 %.

The non-dimensional wall unit (y^+) inside a boundary layer is defined as

$$y^+ = \frac{\rho U_\tau y}{\mu} \tag{10}$$

where $U_\tau \left(= \sqrt{\frac{\tau_w}{\rho}}\right)$ is the friction velocity, τ_w is the wall shear stress, and y is the distance between the first layer of mesh points and the boundary. The maximum y^+ of Mesh-5 is 1.98.

Fig. 4 depicts how the number of released particles affects the estimated deposition efficiency. The deposition rate stays the same as the released particle number is above 157000. The numerical simulations for the present study used the Mesh-5, which has 1.61 million elements and released particle number of 157000.

3.2. Model validation

In our earlier research, we have validated the model in the simulation of TD of micro and nanoparticles (Rahman et al., 2022a; Rahman et al., 2021a). The current CFD approach is validated against published experimental and numerical data of particle deposition in the mouth-throat portion of a lung to further validate the numerical method. The calculated deposition efficiency versus impaction parameter, $d_p^2 Q$ (μm² L/min) for microparticles is presented in Fig. 5 (a), where Q is the volume flow rate together with the experimental data (Bowes and Swift, 1989; Chan and Lippmann, 1980; Cheng et al., 1999; Foord et al., 1978; Lippmann and Albert, 1969; Stahlhofen et al., 1980; Stahlhofen et al., 1983), theoretical results (Emmett et al., 1982), and the numerical results (Kleinstreuer et al., 2008). It is found that the effectiveness of microparticle deposition increases with the increase of the particle size. It is interesting to note that most studies are experimental and have used different samples (Fig. 5a). For example, Lippmann & Abert found deposition efficiency rates with different initial

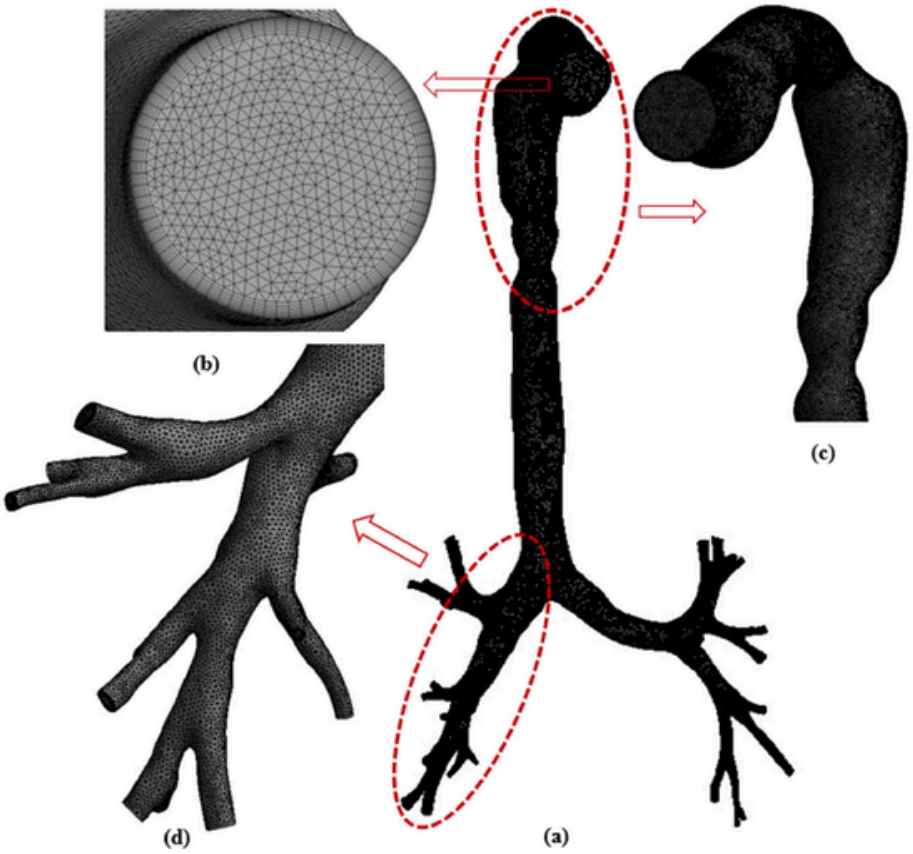

Fig. 2. Realistic lung model mesh for (a) extending from the mouth to 6th generation, (b) Zoomed-in view on mouth surface, (c) Side view of the mouth to larynx region, (d) Zoomed-in view on right side of mesh from G1-G6 generation

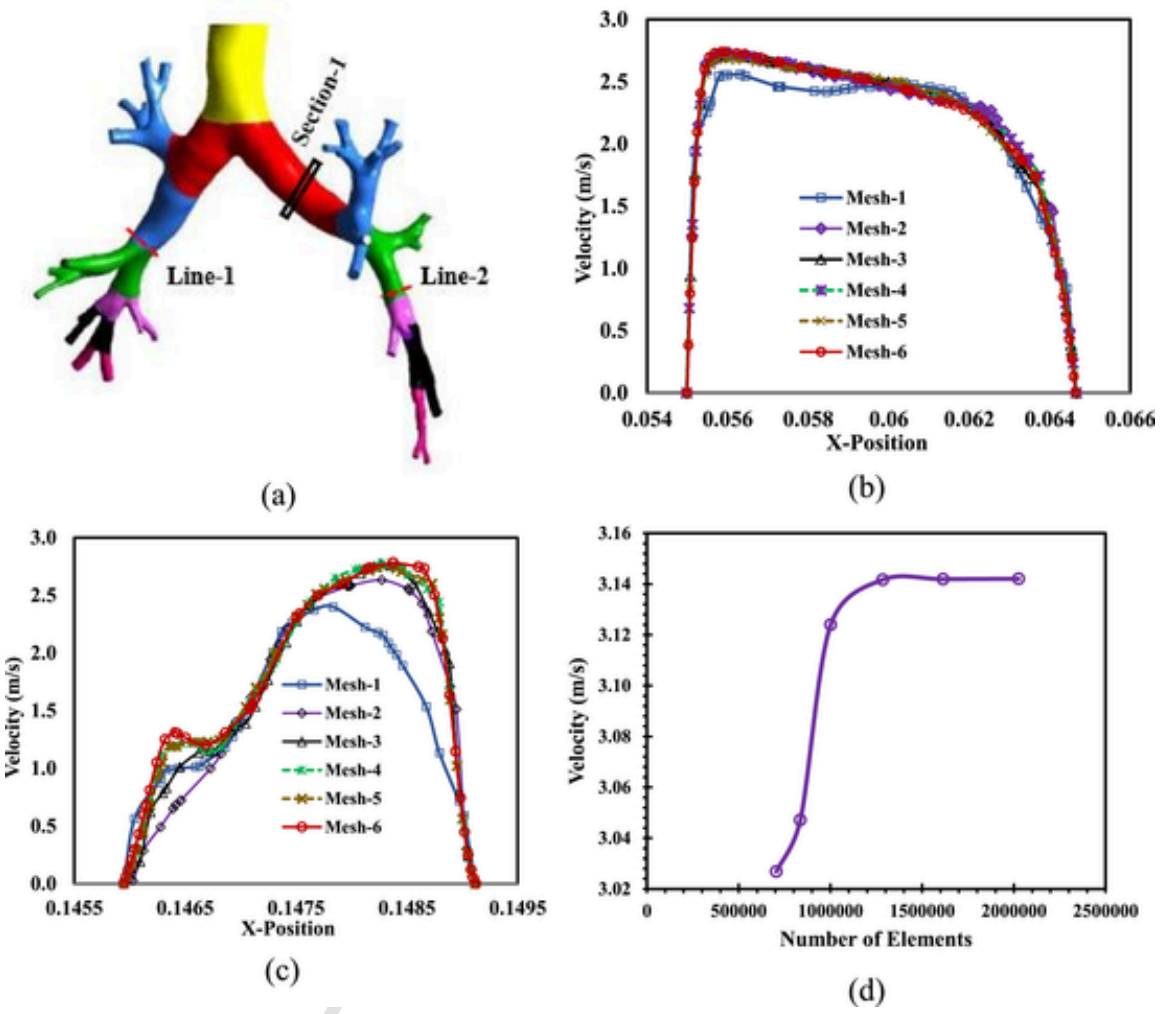

Fig. 3. shows a grid-independency test with a flow rate of 30 L/min, (b) velocity distribution at Line-1, (c) velocity distribution at Line-2, and (d) average velocity vs grid number (average velocity calculated at the selected line and section in Fig. 3a).

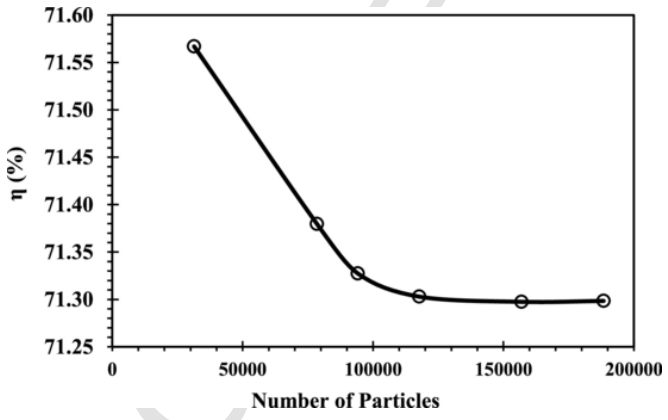

Fig. 4. Deposition efficiency as a function of released particles at the flow rate of 30 L/min in the vertical direction. The diameter and density of smoke particles are 10 μm and 1120 kg/m^3, respectively.

impaction parameters. However, the current studies compared nine (9) published articles based on experimental and numerical measurements with considered two different flow rates and found a limited scattered point. Therefore, the significant deviation for particle deposition efficiency value could be found because everyone used different geometry but the same upper airways. In addition to this, the airway geometry is different for every person, and the mouth-throat section is highly asymmetric. As a result, the deposition efficiency increases in some cases compared to overall deposition efficiency. The present study further investigated to validate nanoparticle deposition in the mouth-throat part at a flow rate $Q = 10$ *L/min* (Fig. 5b). The results match the existing literature Xi and Longest (2008. Hence, the present numerical results agree with the increasing pattern in the microparticle and nanoparticle deposition efficiency with impaction parameters and particle diameter. Fig. 5 shows how the current model can precisely compute the particle TD in a realistic 3D mouth-throat and the tracheobronchial airways of a lung.

4. Results and discussion

This research examines the airflow dynamics and particle deposition under two flow conditions: low activity breathing ($Q = 15$ L/min) at rest and moderate activity breathing ($Q = 30$ L/min) while walking (Rahman et al., 2021c; Zhang et al., 2008).

4.1. Airflow characteristics

Velocity profiles at different points in the mouth-throat to bronchioles regions are compared with one another. Fig. 6 demonstrates the velocity patterns for the two flow rates for four selected cross-sections depicted in Fig. 1 along the diameter direction (X-direction). The velocity

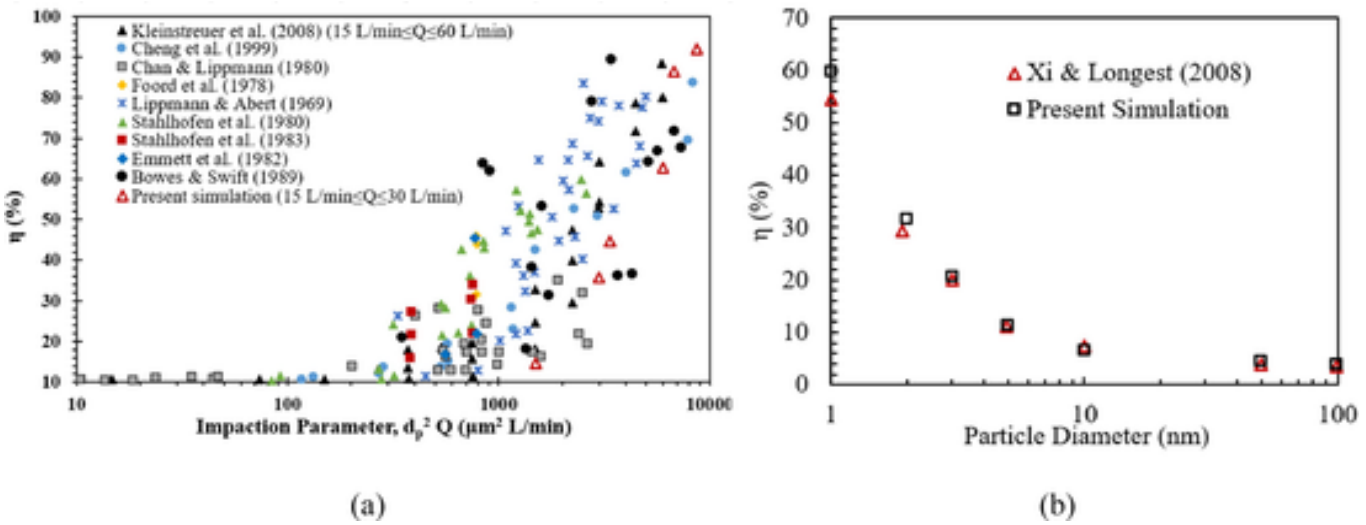

Fig. 5. Comparison of current models of the deposition of (a) microparticles ($1\ \mu\text{m} \le d_p \le 20\ \mu\text{m}$) in the mouth and throat region at the vertical direction and published research (Bowes and Swift, 1989; Chan and Lippmann, 1980; Cheng et al., 1999; Emmett et al., 1982; Foord et al., 1978; Kleinstreuer et al., 2008; Lippmann and Albert, 1969; Stahlhofen et al., 1980; Stahlhofen et al., 1983), and (b) nanoparticles (Xi and Longest, 2008)

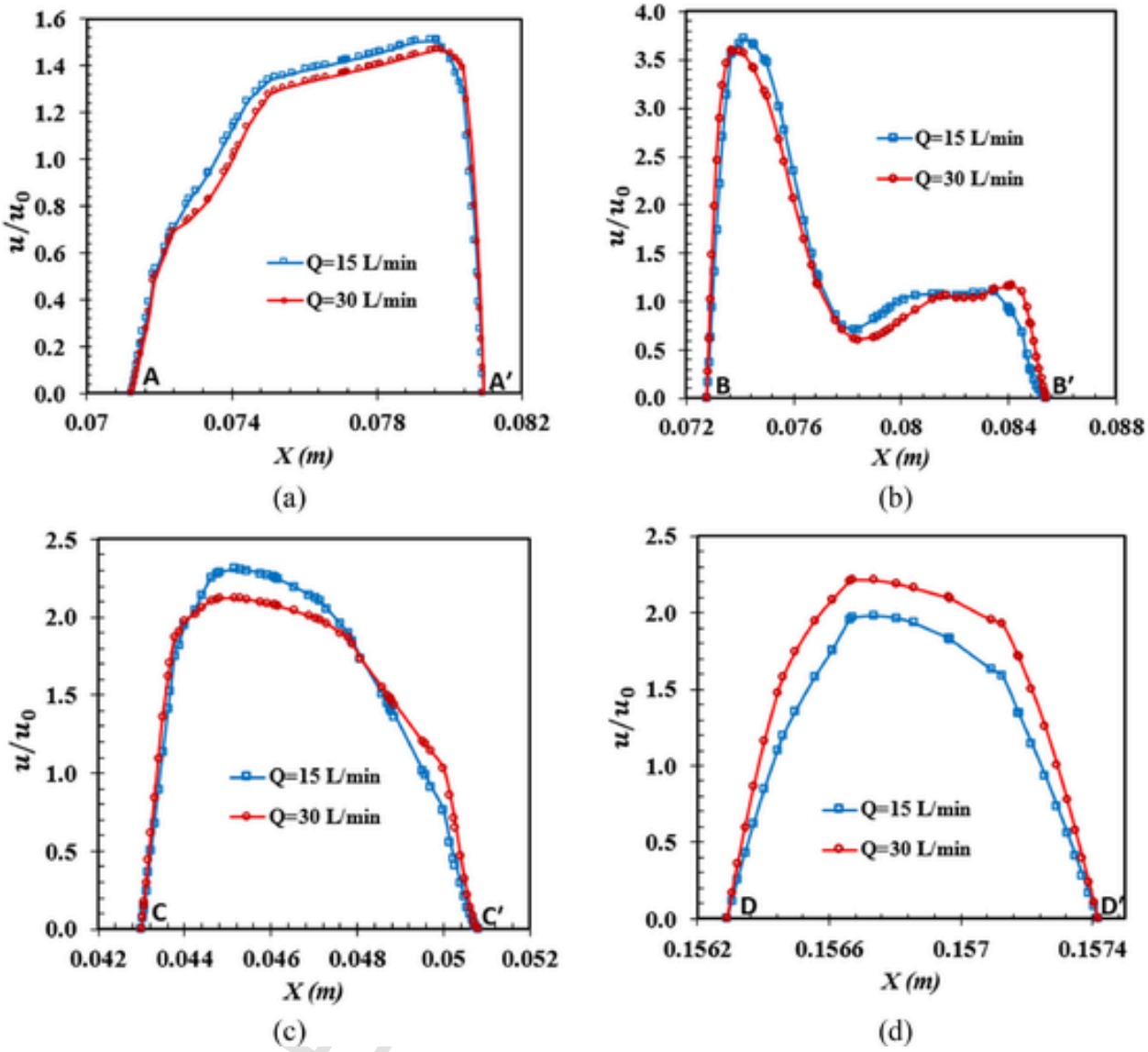

Fig. 6. Velocity profiles under various flow rates, (a) Section AA′, (b) Section BB′, (c) Section CC′, and (d) Section DD′ (Fig. 1 illustrates the sections).

is non-dimensionalised by the inlet velocity of the whole lung model u_0. As soon as the air goes through a bifurcation due to the complexity of the airway geometry, the velocity distribution in each branch becomes very non-uniform. Compared with the mouth-throat and larynx, the lower portions, like the bronchioles, have more complex velocity profiles (Fig. 6a and b). The non-dimensional velocity on portions AA′ and BB′ is consequently more asymmetric. The complexity of the airways in the larynx has a significant impact on section BB′, which is located in the trachea. Sections CC′ and DD′ are situated at the lower portion of the bronchioles, which is why the velocity is uniformly decreased and distributed. As a result, the velocity profile (DD′ section) in the lower trachea shown in Fig. 6d is symmetrical and close to parabolic. Although a comparison of the velocity profiles for the two flow rates of 15 and 30 L/min reveals that non-dimensional velocity distributions have a comparable trend, they are not the same due to the difference in Reynolds number.

To understand the flow field inside the airways and characterise the complex respiratory system passages' flow behaviour. Fig. 7 shows velocity profiles for two flow rates of 15 and 30 L/min. The highest velocity appears to occur in the mouth-throat, larynx, and trachea. From Fig. 7, it can be deduced that the morphology of the airways has a significant impact on the streamlines because it can be observed that the streamlines are highly disordered due to deflections in the flow path in the areas where the airways are more complicated. This occurrence is especially noticeable in the mouth-throat region, where the small passages cause streamlines to be deflected and airflow to circulate inside the maxillary sinuses. In addition, Fig. 7b shows that the flow circulation becomes stronger at a flow rate of 30 L/min. The larynx has been depicted in a magnified view to understand better the streamlines in this region, which is another significant area where the local geometry of the model has a significant impact on the streamlines. Due to a contradiction in the flow cross-section and an increase in flow velocity, the flow through the larynx is suddenly disturbed. However, the flow is disturbed by the local complexity of the geometry.

4.2. Wall shear stress

The averaged non-dimensional shear stress ($\tau/\left(\rho u_0^2\right)$) along the inner wall of the lung is shown quantitatively in Fig. 8 as a function of flow rate in the upper lung airway model on seven sections shown in Fig. 1. Wall shear stress is defined as the tangential force per unit area exerted on the wall surface by the flowing fluid. The highest amount of wall shear occurs on the section 3 bifurcation area of the bronchioles,

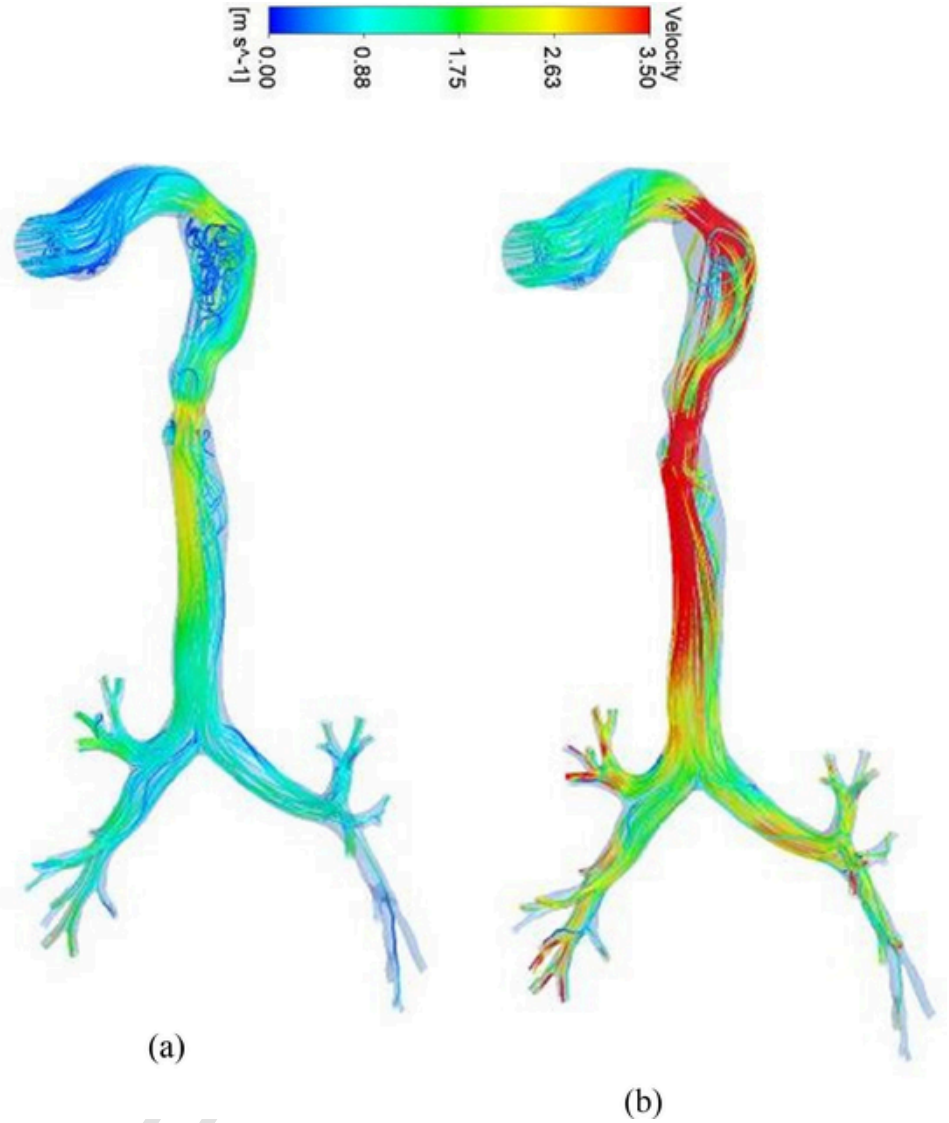

Fig. 7. Velocity streamlines for the different flow rates; (a) $Q = 15$ L/min, and (b) $Q = 30$ L/min.

where the air passes suddenly. Additionally, it has been noted that due to the reduced velocity, there is a significant decrease in wall shear in the bottom part of the right lobe. Due to the complicated lung geometry and resulting flow rate variation, the wall shear stress changes significantly with each section of the lung airway. The relationship between the shear rate and velocity difference is linear. Therefore, Fig. 8 illustrates how a higher flow rate results in a higher velocity difference.

Fig. 9 shows the non-dimensional pressure pass on along the lung airways at various locations, from the mouth to the bronchioles. It has been noted that due to friction with the airway walls and energy loss, the pressure is higher in the mouth-throat area and decreases as it reduces into the lower airways. Due to the combined effects of wall friction and the complex geometry, pressure loss within the airways may occur. The flow would move with high consecutive expansion and contradictions that would affect the pressure as it goes through a complex geometry with narrow passages in certain locations. Therefore, it can be seen that areas with a lot of variation in the cross-section of the airways experience a substantial change in pressure. After the larynx and trachea section, there is a reduction in the airways' cross-section, which results in pressure decreases. As a result, as the flow rate drops, the pressure falls in each section.

4.3. Particle deposition

Traffic, smoke, and dust particles were the three types of pollutants that were examined. Particles come from various sources and vary in size and chemical composition (Kelly and Fussell, 2012). According to the literature, pollutant particles affect the lung the most (Chernyshev et al., 2018). However, whereas particle size has generally been noted as a factor in deposition, the impact of particle chemical composition on TD is through bulk density (Zhao and Castranova, 2011). Hence, we assumed that the density of traffic, smoke, and dust particles is 2000 kg/m^3, 1120 kg/m^3 and 400 kg/m^3, respectively (Deng et al., 2019; Paul et al., 2021). To quantify the contributions of the sedimentation effect, the impaction, Brownian diffusion, and Saffman's lift force using numerical simulations in two scenarios: First, all terms are included in the particle motion equation and inhaled in the sitting or standing position, and second, all terms are included in the particle motion equation and inhaled in the lying down position. We look at the pollutant particles' diameters ranging from 1 μm $\leq d_p \leq$ 10 μm.

The total deposition efficiencies of dust, smoke and traffic particles with different diameters in the lung model shown in Fig. 1 are presented in Fig. 10 for two flow rates of 15 and 30 L/min. The deposition rates of 10 μm particles for different flow rates, particle types and grav-

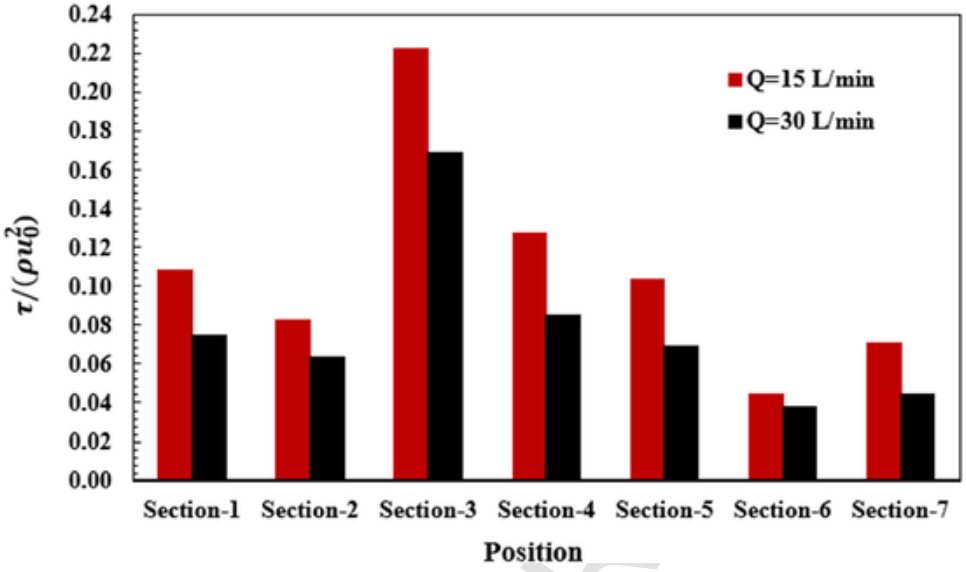

Fig. 8. Averaged wall shear stress for a particular lung portion is indicated in Fig. 1. The smoke particle diameter is 10-μm.

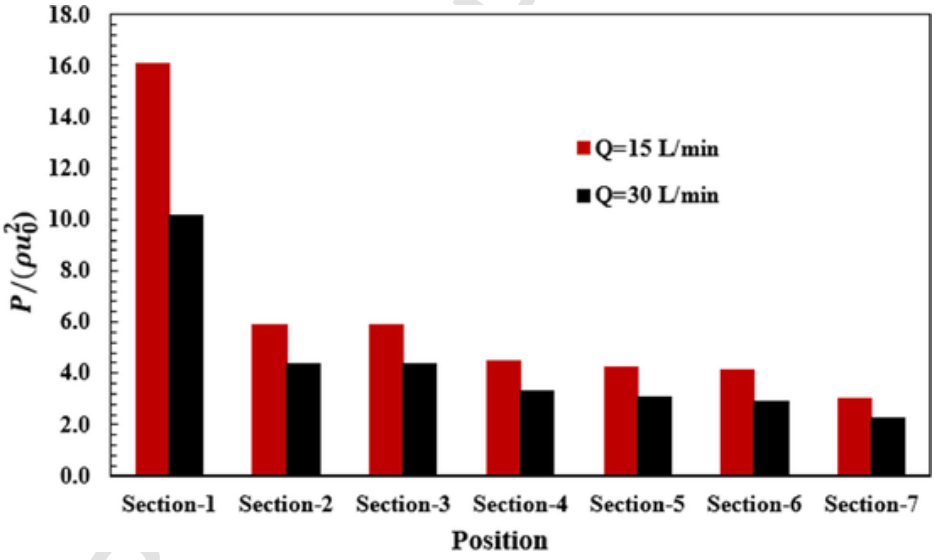

Fig. 9. Averaged pressure at a different section of the lung at distinct flow rates; the section numbers are shown in Fig. 1.

ity directions are listed in Table 1. The deposition rate decreases with the decrease of particle size in the micro-scale because the impaction mechanism weakens (Vachhani and Kleinstreuer, 2021). At a flow rate of 30 L/min, the deposition of 10 μm traffic particles is higher than same-size smoke and dust particles. The inertial effect explains why the deposition rate of macroparticles rises as particle size or flow rate increases. Flow velocity follows the curved airway when it passes through it, but large particles tend to remain on their original tracks due to the inertial mechanism and collide with the airway wall. Inertia impaction is a term used to describe this kind of deposition mechanism (Lippmann and Albert, 1969).

Fig. 10b also shows that by reducing the diameter, the slope of the deposition curve for dust, smoke, and traffic particles becomes nearly similar. The difference between the deposition rates of traffic and dust is 0.411 %, 5.833 % and 52.298 % for 1μm, 5μm and 10 μm particles, respectively. This is because of the low flow rate, the particles follow the fluid streamline, and the impaction mechanisms are weak. Fig. 10a show that at a flow rate of 30 L/min, the deposition rate of traffic particles with various shapes and sizes is higher for similar particles.

In all the simulations, the deposition rate of a horizontal lung is higher than a vertical lung. The difference between the deposition rate of the horizontal lung and vertical lungs is defined as $\Delta\eta = \eta_h - \eta_v$ and shown in Fig. 11. The horizontal lung has higher deposition efficiency because gravity makes more particles deposit on horizontal airways than vertical airways. However, the sedimentation effect is found to be very when the particle size is very small, i.e., 1 μm. If the particle size is greater than 5 μm, the increased contribution of the sedimentation effect makes the vertical and horizontal lungs have a difference in deposition rate. The maximum Δη occurs at the heaviest and largest particles, which are 10 μm traffic particles at 15 L/min and under the smaller flow rate.

The ratio of sedimentation influence in vertical and horizontal is greater than 2 % at the same size of 10 μm traffic particle, indicating that the sedimentation effect is still significant at flow rates of 30 L/min and 15 L/min, respectively. It can be seen that the sedimentation effect increases if the flow rate reduces. When the flow rate is decreased from 30 L/min to 15 L/min, Δη increases for all the particle types and sizes, indicating the contribution of sedimentation increases with the decrease in flow rate.

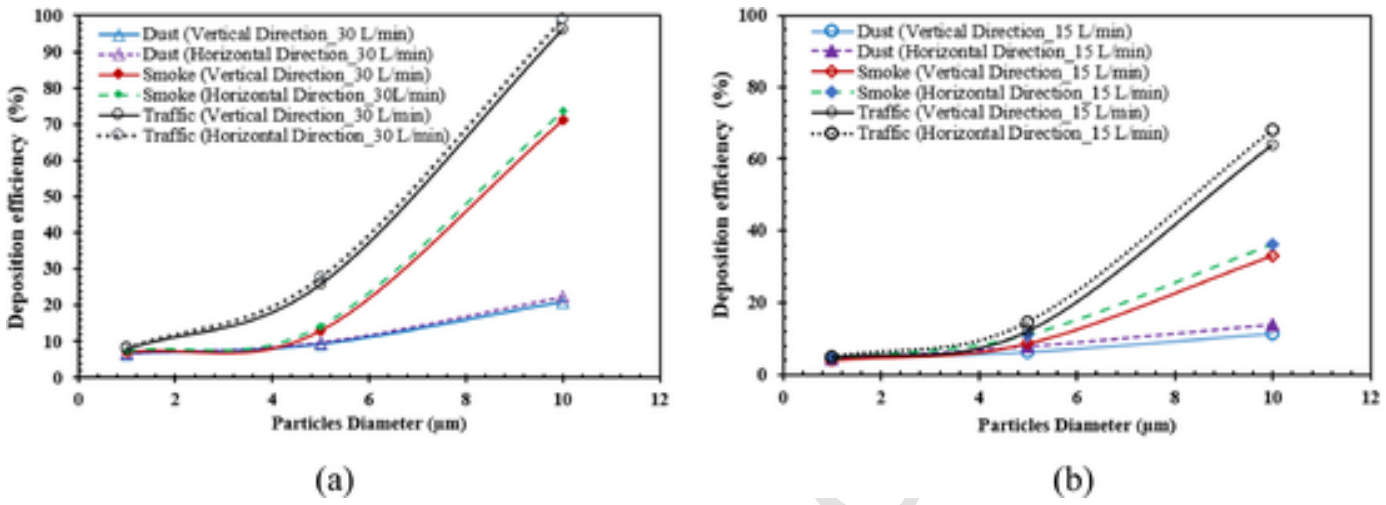

Fig. 10. Particle deposition efficiency in the lung model for (a) $Q = 15$ L/min; (b) $Q = 30$ L/min.

Table 1
Particle deposition rates of the 10 μm particles

Q = 30 L/min			Q = 15 L/min		
Particle type	Gravity direction	Deposition rate (%)	Particle type	Gravity direction	Deposition rate (%)
Dust	V	20.898	Dust	V	11.466
Dust	H	22.345	Dust	H	14.057
Smoke	V	71.297	Smoke	V	33.033
Smoke	H	73.768	Smoke	H	36.111
Traffic	V	96.272	Traffic	V	63.765
Traffic	H	99.098	Traffic	H	68.146

The lung model is divided into parts mouth to bronchioles in Fig. 1, and the distribution of 1-μm dust, smoke, and traffic particles in different parts is demonstrated by the bar charts in Fig. 12. It is found that the deposition rates from the mouth, Larynm and trachea parts are significantly higher than other parts because of the strong impaction and sedimentation effect. The deposition rates of these three parts of the horizontal lung are slightly greater than their counterpart of a vertical lung due to strong sedimentation effects. The deposition rate of dust, smoke, and traffic particle at the mouth-throat area are 1.54 %, 1.68 %, and 1.94 % when the lung is in the horizontal direction. The higher deposition rate of 1-μm traffic particles is observed at the mouth throat area compared to smoke and dust particles because of the density effect. The effect of particle density on other parts and flow rates is also similarly weak.

Fig. 13 depicts the vertical and horizontal deposition rates of 10-μm pollutant (dust, smoke, and traffic) particles at the parts mouth to bronchioles at a flow rate of 30 L/min. At 30 L/min, the deposition efficiency in the mouth-throat area is 96.51 % for 10-μm traffic particles and 25.12 % for 10-μm dust particles. Because of the strongest impact mechanism, the flow rate of 30 L/min causes higher deposition rates than 10 L/min. Because 10-μm traffic particles are mostly deposited at the mouth-throat area at a flow rate of 30 L/min, the deposition efficiencies at the remaining part of the area, from the trachea to 6th generation (G6), are much lower than those of smoke and dust, as shown in Fig. 13 (c). The efficiency of deposition due to impaction increases as particle density increases. Furthermore, impaction results in strong deposition when the airway bends, compresses, or bifurcates. At a flow rate of 30 L/min, some deposition efficiencies of traffic particles are zero at parts G1 to G6 (Fig. 13c) because the majority of the particles are deposited in the mouth-throat region.

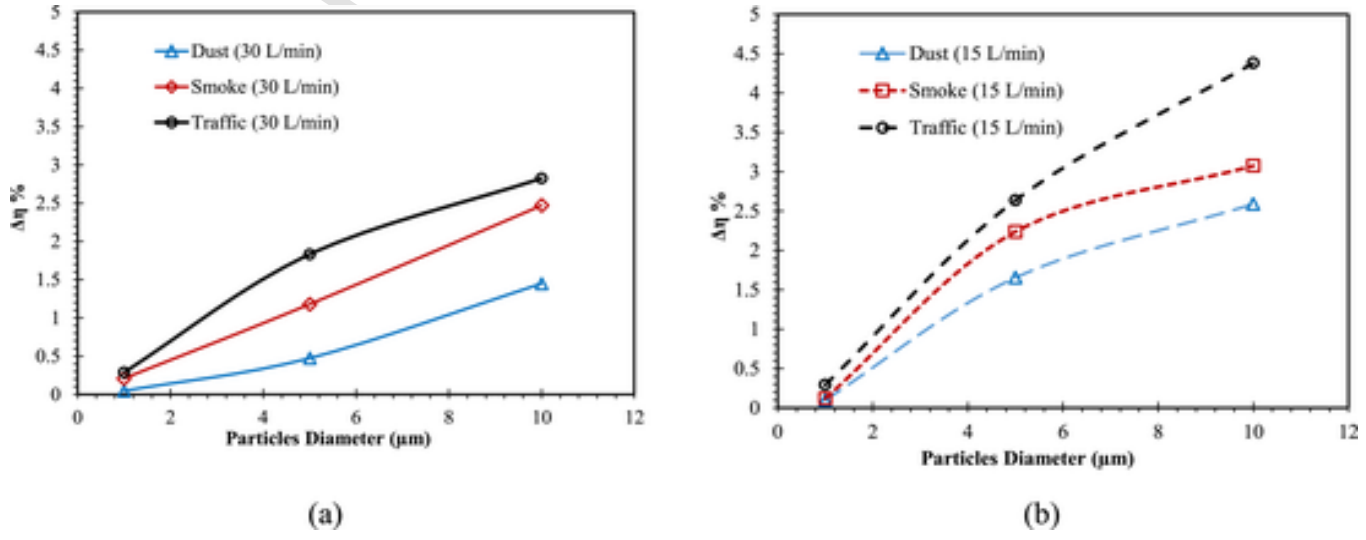

Fig. 11. Difference between the deposition rates of the horizontal and vertical lungs ($\Delta\eta$) as the result of the sediment effect (a) $Q = 30$ L/min; (b) $Q = 15$ L/min

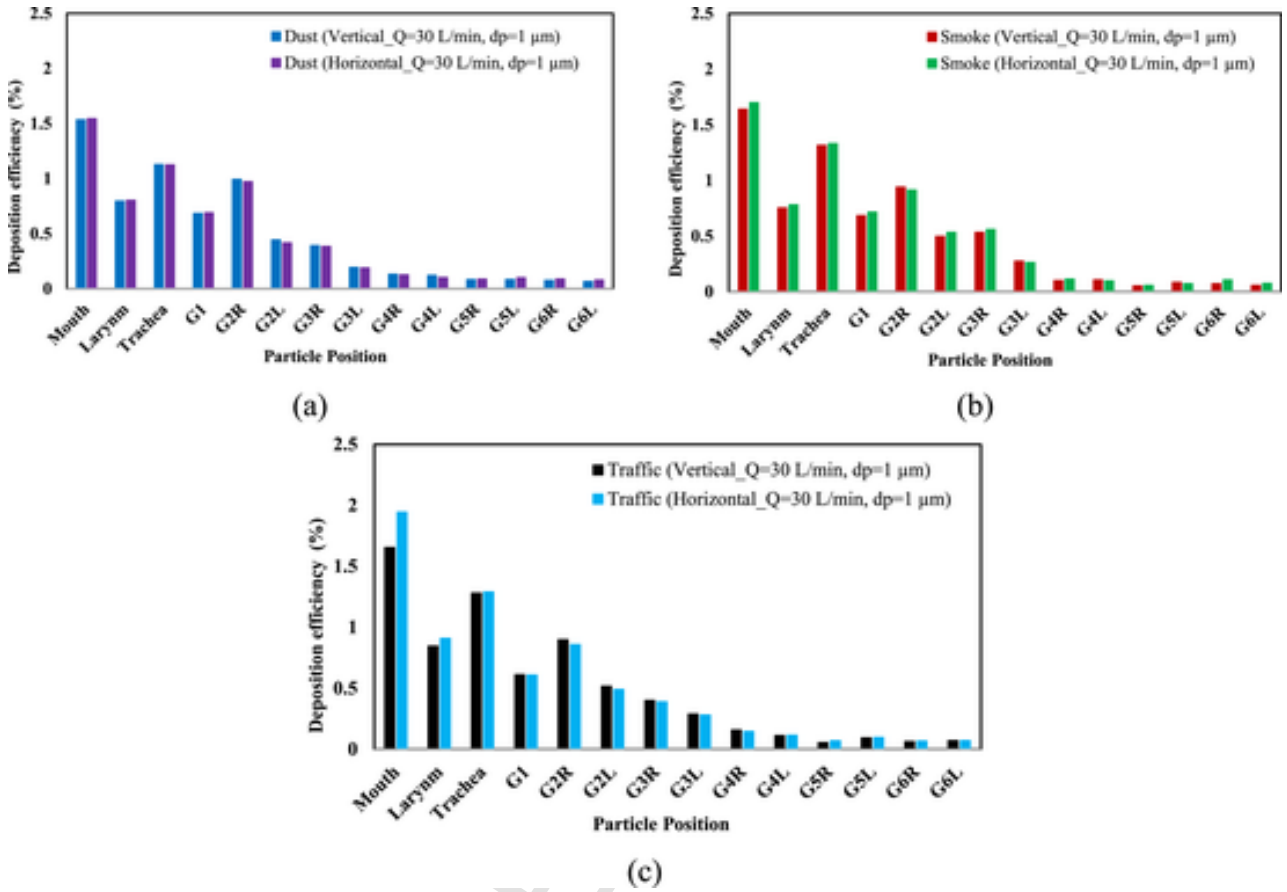

Fig. 12. Deposition efficiencies of 1-μm particles at various parts of the lung (indicated in Fig. 1) at flow rate $Q = 30$ L/min; (a) Dust particle, (b) Smoke particle, (c) Traffic particle.

4.4. Visualisation of particle deposition

Fig. 14 indicate the distribution of deposited dust, smoke and traffic particles at a flow rate of 30 L/min for a vertical lung. These images show that several major hotspots have the highest concentrations of pollutant particle deposition. The mouth-throat, larynx, trachea, and bronchioles are among these locations. At a flow rate of 30 L/min, the mouth-throat region has the highest concentration of pollutant particles. This could be attributed to the dominance of one of the particle deposition mechanisms, inertial impaction. Because particles have inertia when passing through the airways, when the direction of the flow changes, particles with high inertia may be unable to adjust their path with the fluid flow and thus hit the wall. As a result, a large number of 10 m traffic particles are frequently found to be deposited in the mouth-throat region, where the airway is curved, rough, and complex. Because of the repetitive deposition of many particles in the same areas, the quantity of 10 m traffic particles (Fig. 14c) appears to be smaller than that of dust particles (Fig. 14a), but it is not. Approximately 94.51 % of 10 m traffic particles are deposited in the mouth-throat region, with far fewer particles entering the deep airways. Because of the decreased deposition efficiency of 10 μm dust particles in the mouth-throat region, the remaining particles are either deposited in the bifurcation areas or escape and enter the deep lung.

4.5. Particle escaping rate

The percentage of particles that escape from the model's outlet and reach the deep lung is denoted by the escaping rate (η_e). Fig. 15 depicts the escape rates from the Right upper lobe (RUL), Right middle lobe (RML), Right lower lobe (RLL), Left upper lobe (LUL), and Left lower lobe (LLL) for $Q = 30$ L/min in order to understand the distribution of escaped particles among various exits. Fig. 1 depicts all the different exits for each area. The escaping rate of traffic particles in the regions RUL, RML, RLL, LUL, and LLL is nearly zero because the majority of the 10 m traffic particles are deposited in the upper portion at a flow rate of 30 L/min. As a result, the escape rate of 10-μm particles goes up as the particles transform from traffic to dust.

The escaping rate of 10-μm dust particles from the right side (regions RUL, RML & RLL) and left side (regions LUL and LLL) are 53.97 % and 25.01 %, respectively. Similarly, the escaping rate of the smoke particle is 20.94 % on the right side and 7.76 % on the left side, respectively. Therefore, more dust particles escape from both regions and enter the deep lung than smoke and traffic particles. Our research is significant for demonstrating that large size dust particles may also be deposited in the deep lung.

On the other hand, the escaping rate of 5-μm dust, smoke and traffic particles on the right side are 61.57 %, 57.97 %, and 49.67 %, and left side are 30.59 %, 27.68 %, and 22.46 %, respectively. However, when the particle size decreases to 1-μm, the escaping rate does not significantly affect the dust, smoke, and traffic particles. Therefore, dust, smoke, and traffic particles play a significant role in understanding particle transfer and deposition in a human lung.

5. Conclusions

In this study, we have examined the deposition of dust, smoke, and traffic particles in the mouth-throat and tracheobronchial airways at 15 and 30 L/min flow rates. In particular, the sediment effect is investigated by simulating the airflow and particle deposition in the horizontal and vertical lungs. The main findings are summarised as follows:

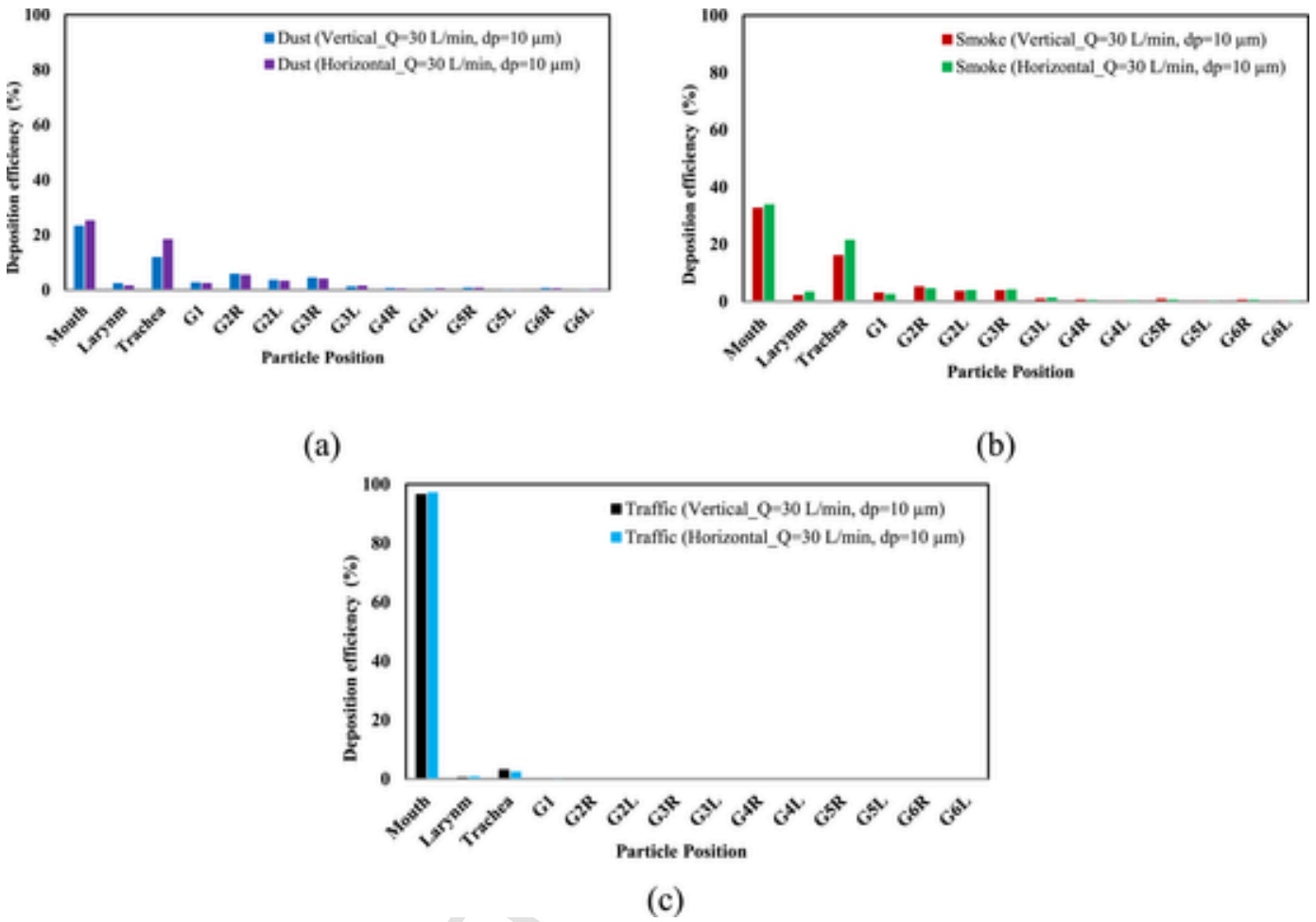

Fig. 13. Deposition efficiencies of 10-μm particles at various parts of the lung (indicated in Fig. 1) at flow rate $Q = 30$ L/min; (a) Dust particle, (b) Smoke particle, (c) Traffic particle.

- The contribution of the sedimentation effect is largely independent of particle size, flow rate and whether the human lung is horizontal or vertical. A horizontal lung has a higher flow rate than a vertical lung. An increase in particle size and an increase in particle density cause an increase in the particle deposition rate.
- 10 μm traffic particles have a higher deposition rate than dust and smoke particles in the human lung airway model because of their higher density.
- The deposition rate of a horizontal lung for the heaviest particles (traffic) at 15 L/min flow rate is about 4.5 % higher than that of a vertical lung with the same flow rate. The difference between the deposition rates of the horizontal and vertical lungs reduces if the particle size reduces, the flow rate increases or the particle density reduces.
- Small-density particles are more evenly distributed in the lung model than heavy-density particles. The deposited dust particles are more evenly distributed in airways than smoke and traffic particles because of the density effect because its density is lighter.
- The density does not affect particle deposition if the particle diameter is relatively small (e.g., 1 μm). As a result, the sedimentation impact of small-size particles is negligible.

The findings of different pollutants particles transport behaviour and their deposition pattern would improve the understanding of the pollutant transport in airways. The findings of the local deposition rate would help to assess the risk associated with different local bronchioles. The conclusions on the effects of the sedimentation can also be used for the development of the more efficient targeted clinical drug delivery through inhalation. This paper conducted a fundamental study under constant flow rates at inlet. It will be extended to the case with varying flow rate that reflects the real breathing pattern.

CRediT author statement

Md. M. Rahman: Conceptualization, Methodology, Writing- Original draft preparation, Validation, formal analysis

Ming Zhao: Methodology, Writing - Review & Editing, Supervision, Resources

Mohammad S. Isla: Writing - Review & Editing

Kejun Dong: Writing - Review & Editing

Suvash C. Saha: Writing - Review & Editing

Declaration of Competing Interest

The authors state no conflict of interest.

Data availability

Data will be made available on request.

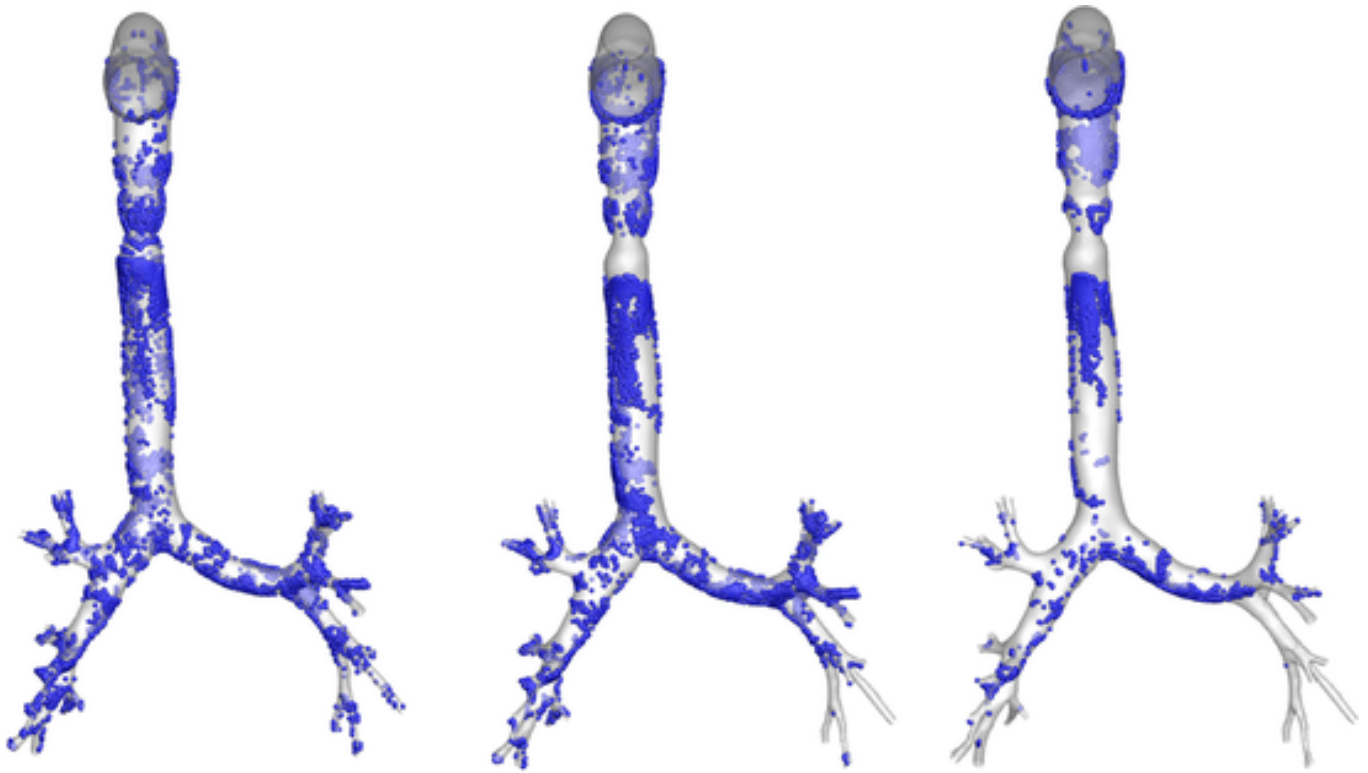

Fig. 14. Distribution of deposited 10-μm particles in the human lung model at a flow rate of 30 L/ min for the vertical direction.

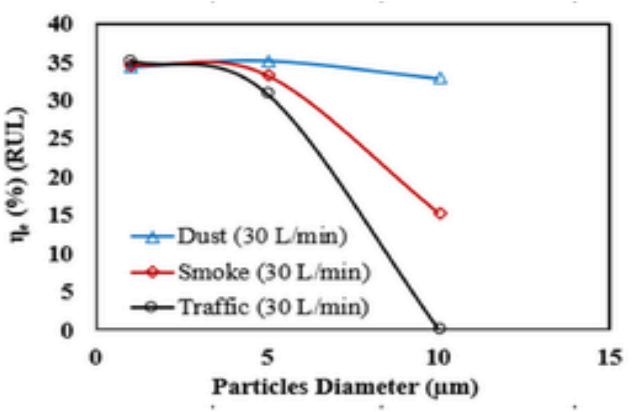
η_e (%) (RUL)
Dust (30 L/min)
Smoke (30 L/min)
Traffic (30 L/min)
Particles Diameter (µm)

(a)

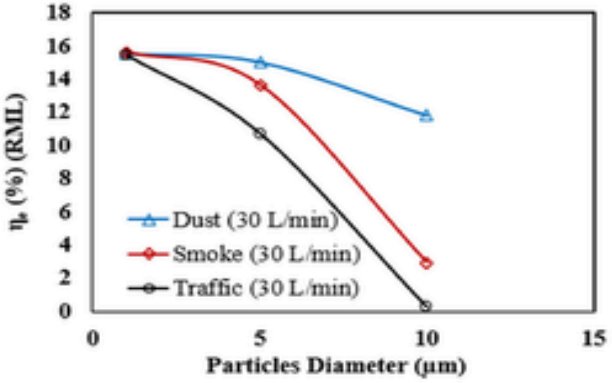
η_e (%) (RML)
Dust (30 L/min)
Smoke (30 L/min)
Traffic (30 L/min)
Particles Diameter (µm)

(b)

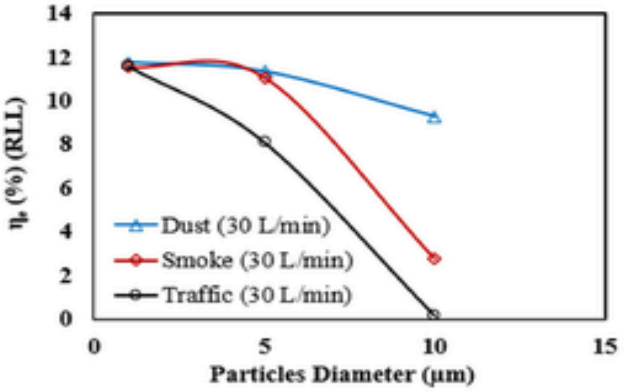
η_e (%) (RLL)
Dust (30 L/min)
Smoke (30 L/min)
Traffic (30 L/min)
Particles Diameter (µm)

(c)

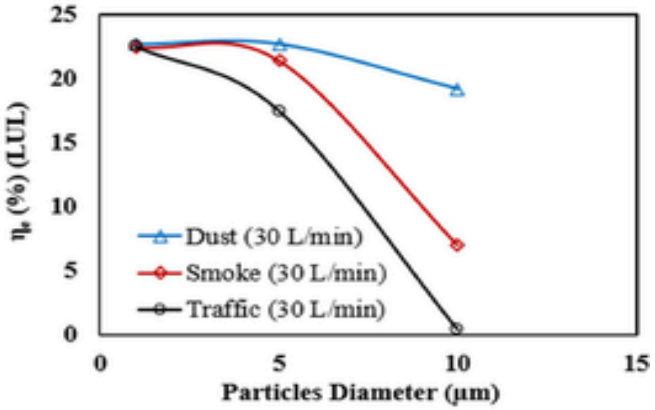
η_e (%) (LUL)
Dust (30 L/min)
Smoke (30 L/min)
Traffic (30 L/min)
Particles Diameter (µm)

(d)

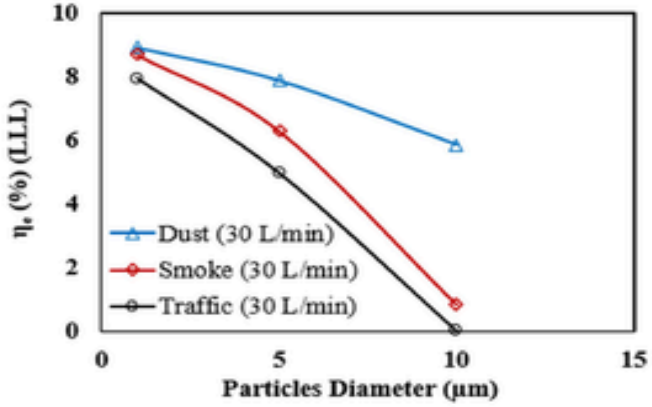
η_e (%) (LLL)
Dust (30 L/min)
Smoke (30 L/min)
Traffic (30 L/min)
Particles Diameter (µm)

(e)

Fig. 15. Escape rate (η_e) for 1 μm ≤ d_p ≤ 10 μm particles at a flow rate 30 **L**/ min: (a) Right upper lobe, (b) Right middle lobe, (c) Right lower lobe, (d) Left upper lobe, and (e) Left lower lobe (Fig. 1 shows the description of all regions).

Acknowledgements

Mr Rahman gratefully acknowledges the International Postgraduate Research Scholarship (IPRS) provided by the Australian Government Research Training Program. The authors also acknowledge that the WSU High-Performance VM machine provided the computational resources.

References

Agarwal, AK, Ateeq, B, Gupta, T, Singh, AP, Pandey, SK, Sharma, N, et al., 2018. Toxicity and mutagenicity of exhaust from compressed natural gas: Could this be a clean solution for megacities with mixed-traffic conditions? Environ. Pollut. 239, 499–511.
Bowes, III, SM, Swift, DL, 1989. Deposition of inhaled particles in the oral airway during oronasal breathing. Aerosol Sci. Technol. 11, 157–167.
Chan, TL, Lippmann, M., 1980. Experimental measurements and empirical modelling of the regional deposition of inhaled particles in humans. Am. Ind. Hyg. Assoc. J. 41, 399–409.
Chen, R, Hu, B, Liu, Y, Xu, J, Yang, G, Xu, D, et al., 2016. Beyond PM2. 5: The role of ultrafine particles on adverse health effects of air pollution. Biochimica et Biophysica Acta (BBA)-General Subj. 1860, 2844–2855.
Cheng, Y-S, Zhou, Y, Chen, BT., 1999. Particle deposition in a cast of human oral airways. Aerosol Sci. Technol. 31, 286–300.
Chernyshev, V, Zakharenko, A, Ugay, S, Hien, T, Hai, L, Kholodov, A, et al., 2018. Morphologic and chemical composition of particulate matter in motorcycle engine exhaust. Toxicol. Rep. 5, 224–230.
Darquenne, C., 2020. Deposition mechanisms. J. Aerzosol Med. Pulmon. Drug Deliv. 33, 181–185.
Deng, Q, Deng, L, Miao, Y, Guo, X, Li, Y., 2019. Particle deposition in the human lung: health implications of particulate matter from different sources. Environ. Res. 169, 237–245.
Deng, Q, Ou, C, Chen, J, Xiang, Y., 2018. Particle deposition in tracheobronchial airways of an infant, child and adult. Sci. Total Environ. 612, 339–346.
Derbyshire, E., 2007. Natural minerogenic dust and human health. AMBIO: A J. Hum. Environ. 36, 73–77.
Dockery, DW, Pope, CA., 1994. Acute respiratory effects of particulate air pollution. Annu. Rev. Public Health 15, 107–132.
Emmett, P, Aitken, R, Hannan, W., 1982. Measurements of the total and regional deposition of inhaled particles in the human respiratory tract. J. Aerosol Sci. 13, 549–560.
Farkas, Á, Füri, P, Thén, W, Salma, I., 2022. Effects of hygroscopic growth of ambient urban aerosol particles on their modelled regional and local deposition in healthy and COPD-compromised human respiratory system. Sci. Total Environ. 806, 151202.
Farnoud, A, Tofighian, H, Baumann, I, Garcia, GJ, Schmid, O, Gutheil, E, et al., 2020. Large eddy simulations of airflow and particle deposition in pulsating bi-directional nasal drug delivery. Phys. Fluid. 32.
Foord, N, Black, A, Walsh, M., 1978. Regional deposition of 2.5–7.5 μm diameter inhaled particles in healthy male non-smokers. J. Aerosol Sci. 9, 343–357.
Interventional, Aso, Neuroradiology, T, Angiography, SfC, Interventions, Medicine, SfV, Biology, et al., 2007. ACCF/SCAI/SVMB/SIR/ASITN 2007 clinical expert consensus document on carotid stenting: a report of the American College of Cardiology foundation task force on clinical expert consensus documents (ACCF/SCAI/SVMB/SIR/ASITN clinical expert consensus document committee on carotid stenting). J. Am. Coll. Cardiol. 49, 126–170.
Inthavong, K, Ge, Q, Se, CM, Yang, W, Tu, J., 2011. Simulation of sprayed particle deposition in a human nasal cavity including a nasal spray device. J. Aerosol Sci. 42, 100–113.
Islam, MS, Fang, T, Oldfield, C, Larpruenrudee, P, Beni, HM, Rahman, MM, et al., 2022a. Heat wave and bushfire meteorology in New South Wales, Australia: air quality and health impacts. Int. J. Environ. Res. Public Health 19, 10388.
Islam, MS, Rahman, MM, Arsalanloo, A, Beni, HM, Larpruenrudee, P, Bennett, NS, et al., 2022b. How SARS-CoV-2 Omicron droplets transport and deposit in realistic extrathoracic airways. Phys. Fluid. 34, 113320.
Kelly, FJ, Fussell, JC., 2012. Size, source and chemical composition as determinants of toxicity attributable to ambient particulate matter. Atmos. Environ. 60, 504–526.
Kleinstreuer, C, Zhang, Z., 2003. Laminar-to-turbulent fluid-particle flows in a human airway model. Int. J. Multiph. Flow 29, 271–289.
Kleinstreuer, C, Zhang, Z., 2010. Airflow and particle transport in the human respiratory system. Annu. Rev. Fluid Mech. 42, 301–334.
Kleinstreuer, C, Zhang, Z, Kim, CS., 2007. Combined inertial and gravitational deposition of microparticles in small model airways of a human respiratory system. J. Aerosol Sci. 38, 1047–1061.
Kleinstreuer, C, Zhang, Z, Li, Z, Roberts, WL, Rojas, C., 2008. A new methodology for targeting drug-aerosols in the human respiratory system. Int. J. Heat Mass Transfer 51, 5578–5589.
Kuga, K, Kizuka, R, Khoa, ND, Ito, K., 2023. Effect of transient breathing cycle on the deposition of micro and nanoparticles on respiratory walls. Comput. Methods Programs Biomed. 107501.
Kyung, SY, Jeong, SH., 2020. Particulate-matter related respiratory diseases. Tubercul. Respirat. Dis. 83, 116.
Lee, H-G, Kim, D-W, Park, C-W., 2018. Dry powder inhaler for pulmonary drug delivery: human respiratory system, approved products and therapeutic equivalence guideline. J. Pharmaceut. Investig. 48, 603–616.
Lippmann, M, Albert, RE., 1969. The effect of particle size on the regional deposition of inhaled aerosols in the human respiratory tract. Am. Ind. Hyg. Assoc. J. 30, 257–275.
Naseri, A, Abouali, O, Ghalati, PF, Ahmadi, G., 2014. Numerical investigation of regional particle deposition in the upper airway of a standing male mannequin in calm air surroundings. Comput. Biol. Med. 52, 73–81.
Naseri, A, Shaghaghian, S, Abouali, O, Ahmadi, G., 2017. Numerical investigation of transient transport and deposition of microparticles under unsteady inspiratory flow in human upper airways. Respir. Physiol. Neurobiol. 244, 56–72.
Nomura, S, Sakamoto, H, Ghaznavi, C, Inoue, M., 2022. Toward a third term of Health Japan 21–implications from the rise in non-communicable disease burden and highly preventable risk factors. Lancet Region. Health-West. Pacif. 21, 100377.
Oravisjärvi, K, Pietikäinen, M, Ruuskanen, J, Rautio, A, Voutilainen, A, Keiski, RL., 2011. Effects of physical activity on the deposition of traffic-related particles into the human lungs in silico. Sci. Total Environ. 409, 4511–4518.
Organization WHO, 2009. Global Health Risks: Mortality and Burden of Disease Attributable to Selected Major Risks. World Health Organization.
Paul, AR, Khan, F, Jain, A, Saha, SC., 2021. Deposition of smoke particles in human airways with realistic waveform. Atmosphere 12, 912.
Pourmehran, O, Arjomandi, M, Cazzolato, B, Tian, Z, Vreugde, S, Javadiyan, S, et al., 2021. Acoustic drug delivery to the maxillary sinus. Int. J. Pharm. 606, 120927.
Pourmehran, O, Cazzolato, B, Tian, Z, Arjomandi, M., 2020. Acoustically-driven drug delivery to maxillary sinuses: aero-acoustic analysis. Eur. J. Pharm. Sci. 151, 105398.
Pourmehran, O, Gorji, TB, Gorji-Bandpy, M., 2016. Magnetic drug targeting through a realistic model of human tracheobronchial airways using computational fluid and particle dynamics. Biomech. Model. Mechanobiol. 15, 1355–1374.
Rahimi-Gorji, M, Gorji, TB, Gorji-Bandpy, M., 2016. Details of regional particle deposition and airflow structures in a realistic model of human tracheobronchial airways: two-phase flow simulation. Comput. Biol. Med. 74, 1–17.
Rahimi-Gorji, M, Pourmehran, O, Gorji-Bandpy, M, Gorji, T., 2015. CFD simulation of airflow behavior and particle transport and deposition in different breathing conditions through the realistic model of human airways. J. Mol. Liq. 209, 121–133.
Rahman, M, Zhao, M, Islam, MS, Dong, K, Saha, SC., 2022a. Numerical study of nano and micro pollutant particle transport and deposition in realistic human lung airways. Powder Technol. 402, 117364.
Rahman, MM, Zhao, M, Islam, MS, Dong, K, Saha, SC., 2021a. Aging effects on airflow distribution and micron-particle transport and deposition in a human lung using CFD-DPM approach. Adv. Powder Technol. 32, 3506–3516.
Rahman, MM, Zhao, M, Islam, MS, Dong, K, Saha, SC., 2021b. Aging effects on airflow distribution and micron-particle transport and deposition in a human lung using CFD-DPM approach. Adv. Powder Technol. 32, 3506–3516.
Rahman, MM, Zhao, M, Islam, MS, Dong, K, Saha, SC., 2021c. Numerical study of nanoscale and microscale particle transport in realistic lung models with and without stenosis. Int. J. Multiph. Flow 145, 103842.
Rahman, MM, Zhao, M, Islam, MS, Dong, K, Saha, SC., 2022b. Nanoparticle transport and deposition in a heterogeneous human lung airway tree: An efficient one path model for CFD simulations. Eur. J. Pharm. Sci. 177, 106279.
Stahlhofen, W, Gebhart, J, Heyder, J., 1980. Experimental determination of the regional deposition of aerosol particles in the human respiratory tract. Am. Ind. Hyg. Assoc. J. 41, 385–398a.
Stahlhofen, W, Gebhart, J, Heyder, J, Scheuch, G., 1983. New regional deposition data of the human respiratory tract. J. Aerosol Sci. 14, 186–188.
Tekatli, H, Haasbeek, N, Dahele, M, De Haan, P, Verbakel, W, Bongers, E, et al., 2016. Outcomes of hypofractionated high-dose radiotherapy in poor-risk patients with "ultracentral" non–small cell lung cancer. J. Thorac. Oncol. 11, 1081–1089.
Thakur, AK, Chellappan, DK, Dua, K, Mehta, M, Satija, S, Singh, I., 2020. Patented therapeutic drug delivery strategies for targeting pulmonary diseases. Expert Opin. Ther. Pat. 30, 375–387.
Tretiakow, D, Tesch, K, Meyer-Szary, J, Markiet, K, Skorek, A., 2021. Three-dimensional modeling and automatic analysis of the human nasal cavity and paranasal sinuses using the computational fluid dynamics method. Eur. Arch. Otorhinolaryngol. 278, 1443–1453.
Vachhani, S, Kleinstreuer, C., 2021. Comparison of micron-and nano-particle transport in the human nasal cavity with a focus on the olfactory region. Comput. Biol. Med. 128, 104103.
Valavanidis, A, Fiotakis, K, Vlachogianni, T., 2008. Airborne particulate matter and human health: toxicological assessment and importance of size and composition of particles for oxidative damage and carcinogenic mechanisms. J. Environ. Sci. Health, Part C 26, 339–362.
Verhoeven, JI, Allach, Y, Vaartjes, IC, Klijn, CJ, de Leeuw, F-E., 2021. Ambient air pollution and the risk of ischaemic and haemorrhagic stroke. Lancet Planet Health 5, e542–e552.
Wong, W, Fletcher, DF, Traini, D, Chan, H-K, Young, PM., 2012. The use of computational approaches in inhaler development. Adv. Drug. Deliv. Rev. 64, 312–322.
Xi, J, Longest, PW., 2008. Effects of Oral Airway Geometry Characteristics on the Diffusional Deposition of Inhaled Nanoparticles.
Zhang, Z, Kleinstreuer, C, Kim, C., 2002. Micro-particle transport and deposition in a human oral airway model. J. Aerosol Sci. 33, 1635–1652.
Zhang, Z, Kleinstreuer, C, Kim, CS., 2008. Airflow and nanoparticle deposition in a 16-generation tracheobronchial airway model. Ann. Biomed. Eng. 36, 2095–2110.

Zhao, J, Castranova, V., 2011. Toxicology of nanomaterials used in nanomedicine. J. Toxicol. Environ. Health, Part B 14, 593–632.